RESEARCH ARTICLE

WILEY

Predicting the seismic behavior of multiblock tower structures using the level set discrete element method

John M. Harmon[1] | **Vahe Gabuchian**[2] | **Ares J. Rosakis**[2] | **Joel P. Conte**[3] 🟢 | **José I. Restrepo**[3] | **Andrés Rodriguez**[3] | **Arpit Nema**[4] | **Andrea R. Pedretti**[5] | **José E. Andrade**[1] 🟢

[1]Mechanical and Civil Engineering, California Institute of Technology, Pasadena, California, USA

[2]Graduate Aerospace Laboratories, California Institute of Technology, Pasadena, California, USA

[3]Department of Structural Engineering, University of California, San Diego, California, USA

[4]Pacific Earthquake Engineering Research Center, University of California, Richmond, California, USA

[5]CTO, Energy Vault, Inc., Westlake Village, California, USA

Correspondence
José E. Andrade, Professor, Mechanical and Civil Engineering, California Institute of Technology, 1200 E California Blvd. Pasadena, CA, USA.
Email: jandrade@caltech.edu

Funding information
Energy Vault, Inc

Abstract

In this paper a modeling method is validated at multiple scales for the seismic performance of multiblock tower structure (MTS). MTS are a proposed concept for large-capacity gravitational energy storage that will enable renewable energy sources. The structure modeled is a tower of 7144 nominally identical blocks arranged in a 38-layered annular pattern with no adhesive mechanisms between the blocks or the blocks and the foundation. The level set discrete element method is used to model the dynamics of the tower structure experiencing a ground motion. Experimental determination of each model parameter is shown from the use of individual blocks before construction. Close comparisons to experimental results are shown for the dynamic motion of the tower over a full ground motion time history for multiple scales, materials and ground motions. When the tower was brought to failure, the two ground motions used produced distinct failure modes of the tower showing both a peeling and buckling behavior. Both the effect of the friction coefficient and unequal block heights are investigated. Friction coefficient has a noticeable effect on the amplitude of motion of the tower while the unevenness of the block heights affects mostly the structural speed.

KEYWORDS
discrete element modeling, discrete structures, friction, seismic behavior

1 | INTRODUCTION

The development of green energies, such as solar and wind, is being aggressively pursued in order to meet global goals of CO_2 reduction.[1] The production of these green energies is intermittent, however, and therefore require large scale energy storage to provide continuous energy.[2] Currently, energy storage consists mainly of pumped hydropower storage which comprises 93% of the large scale storage.[3] Energy Vault, Inc. looks to continue to utilize gravity storage using solid blocks in the form of a multiblock tower structure (MTS) instead of liquid water as the material holding the potential energy. MTS is a structural concept where many blocks are stacked together relying on friction as the source of energy dissipation, breaking away from conventional methods for providing seismic resistance.

The field of masonry is one of the closest analogs to MTS due to each being fundamentally composed of stacked discrete blocks. A large portion of computer methods in the field of seismic resistance of masonry structures have been

NOVELTY

- This paper numerically models the earthquake dynamics of multiblock tower structures intended for energy storage use for the first time.
- The level set version of the discrete element method is used for the first time in the field of structural dynamics.
- Validation of the level set discrete element method for multiblock tower structures is conducted for multiple tower materials and scales experiencing multiple ground motions.
- The effects of friction and block height variability are numerically investigated for multiblock tower structures.
- To this point, the level set discrete element method calibrated parameters, such as stiffness, but here they are determined experimentally.

focused on continuum modeling of masonry walls. Continuum modeling makes sense because masonry walls have mortar between blocks instead of the frictional contact between the blocks for MTS. In these continuum models the mortar is often represented using elements with a damage variable that describes cracking or crushing.[4–8]

In order to model these novel structures that feature a large amount of strictly frictional contacts, a discrete element model is developed and validated in this paper instead of a continuum model. The discrete element method (DEM) is a modeling technique that has been used to understand the mechanics of discrete systems where the kinematics and contacts of each element is of much greater consequence than the deformation of that element.[9] The advantage of DEM comes from the efficient modeling of contact and motion due to making a rigid body assumption on its discrete elements. This has put DEM as the method of choice for materials that undergo large, non-linear deformations that are a result of complex microstructures. Examples of this include sand experiencing shear failure, fracture propagation in rock, and fault gouge modeling.[10–13] Each of these examples have microstructures that can be described by grains or particles (the "elements") interacting with one another.

The development of DEM has largely focused on improving the ability to model complex shapes of each element. Initially, elements were only circles (for 2D analysis) or spheres (for 3D analysis) but over time elements evolved to be described by clumped spheres, polyhedrons, Fourier descriptors, splines, and level sets among others.[14–18] Here we choose the level set version because level sets can describe any shape. LS-DEM has previously been validated as predictive for sands[10]; however this is the first time it has been used for modeling and response simulation of structures. In this study, only a simple block shape is used, but the ability to describe any shape allows for more options in future development of MTS.

DEM has been used before in structural mechanics. DEM is also often used in the field of masonry where joints connect faces, edges, and vertices together and are assigned brittle constitutive behavior to simulate the mortar.[19–21] Beyond masonry however, DEM has also found another use in structural mechanics and that is for studying multidrum columns on ancient structures such as those in Greece and Rome.[22,23] Multidrum columns are built in layers, where a single column consists of many cylindrical sections stacked on top of each other without mortar in between. Due to the construction method, the column must rely on friction to provide stability. Many multidrum column structures are still standing in seismic regions after thousands of years, highlighting the seismic resilience potential of friction mechanisms.

For a MTS, energy dissipation relies on the rocking and sliding of the blocks, similar to these ancient structures that survived up to this day. To investigate their seismic performance, a complete modeling suite consisting of theory, numerical simulation and experiments at different scales has been completed.[24] This paper will focus on and detail the numerical modeling performed within the larger study.

First, an overview of the research campaign conducted beyond the numerical modeling will be presented. LS-DEM as a method will then be summarized with some important notes on the differences for this application. Then we will discuss how each parameter in the model was determined using simple experiments. An important section is provided to describe the numerical specimen preparation for realistic modeling of the towers. Finally, results from the numerical model will be presented and discussed along with experimental validation for multiple scales, materials, and ground motions.

2 | TOWER DESIGN AND EXPERIMENTAL CAMPAIGN

The chosen tower design features 7144 nominally identical blocks arranged in 38 layers of 188 blocks each. At full scale, the block dimensions are 1.36 m by 2.82 m by 4.25 m for length, width and height, respectively. For feasibility of

TABLE 1 Details for the ground motions used.

Location	Magnitude	PGA	PGV
Ridgecrest	7.1 Mw	0.511 g	42.4 cm/s
Denali	7.9 Mw	0.33 g	161.8 cm/s

experimental modeling and testing, the tower was scaled down to two different length scales. The proper scaling method for MTS is called μ-scaling which was developed specifically for frictional structures subjected to primarily sliding types of deformation.[25] This scaling was derived from Buckingham's Pi Theorem and requires that to maintain similarity, the dimensionless number, μ^N, must remain the same between the model and the prototype. The dimensionless number μ^N is defined by,

$$\mu^N = \frac{\upsilon}{\sqrt{\ell \mu g}} = constant \tag{1}$$

where υ is velocity, ℓ is a characteristic length, μ is the friction coefficient and g is gravity. The scaling factor between the model and the prototype is denoted as $\lambda_x (= x^M / x^P)$, for any variable x. In terms of λ, the μ-scaling results is the following for time, velocity and acceleration.

$$\lambda_t = \sqrt{\lambda_\ell / \lambda_\mu} \tag{2}$$

$$\lambda_\upsilon = \sqrt{\lambda_\ell \lambda_\mu} \tag{3}$$

$$\lambda_a = \lambda_\ell \tag{4}$$

where t is time and a is acceleration. This scaling is a more general form than the Froude number scaling, with the Froude number scaling being equal to the μ-number scaling in the special case when the model and prototype friction coefficients are the same. Note that mass does not intervene in both of these similitude theories[25] and the experimental testing shows that this is the case.[26]

Experiments and predictions in this paper are μ-scaled from a full height tower made of concrete blocks. The aluminum towers, however, are Froude scaled as the μ-number theory had not been fully developed at that time.

Figure 1 shows the built tower both in experiment (physical models) and virtually (numerical model) from the top and the front. The arrangement of blocks in each layer, which can be seen from the top view, is called the tiling of the layer. Each layer uses a tiling configuration corresponding to a 90 degree rotation of the previous layer. The tiling has a two-fold rotational symmetry so that every other layer is identical. The tiling is specifically designed so the blocks exhibit a high degree of interlocking with the intention of improving the stability of the tower. The tiling was designed so that no two blocks above or below each other are aligned, and the blocks are sized such that each block is resting above exactly two blocks underneath. The tiling pattern is the same for all tower specimens. The figure also shows close ups of the blocks themselves. Digital image correlation (DIC) was used to measure the motion of the towers so dots were painted on the blocks to improve the correlations. The aluminum tower was also painted to enable DIC measurements.

The full campaign was composed of two phases where tower specimens for each phase were built at different scales. In phase 1, towers of either wood or aluminum blocks were built at Caltech at $\lambda_\ell = 1/107$ length scale. A total of five such towers were constructed and fourteen uni-axial tests were conducted across all towers. Details of this experimental campaign can be accessed in Gabuchian et al.[26] Phase 2 was conducted at the UC Berkeley PEER Center shake table on tower specimens at $\lambda_\ell = 1/25$ scale with blocks made of concrete. A total of three towers were built with seven uni-axial and tri-axial tests being applied between them over the course of this phase. For details on phase 2 please refer to Restrepo et al.[27] A paper providing an overview of the entire research campaign was published by Andrade et al.[24]

Two distinct earthquake ground motions were used repeatedly during testing at both scales shown in Table 1. One was recorded at China Lake Station during the 7.1 M_w Ridgecrest Earthquake on July 5, 2019, in California. This station was 3.5 km from the fault, recorded a peak ground acceleration of 0.51 g, and a peak ground velocity of 42.4 cm/s. The other is a ground motion from the 7.9 M_w Denali earthquake on November 3, 2002, in Alaska. This ground motion has a peak ground acceleration of 0.33 g and a peak ground velocity of 161.8 cm/s. The Denali earthquake is notable due to the rupture speed exceeding the shear wave speed, a phenomenon often described as super-shear. For this paper, we will be using the experimental measurements from a subset of the tests completed. The chosen measurements will be from tests on towers
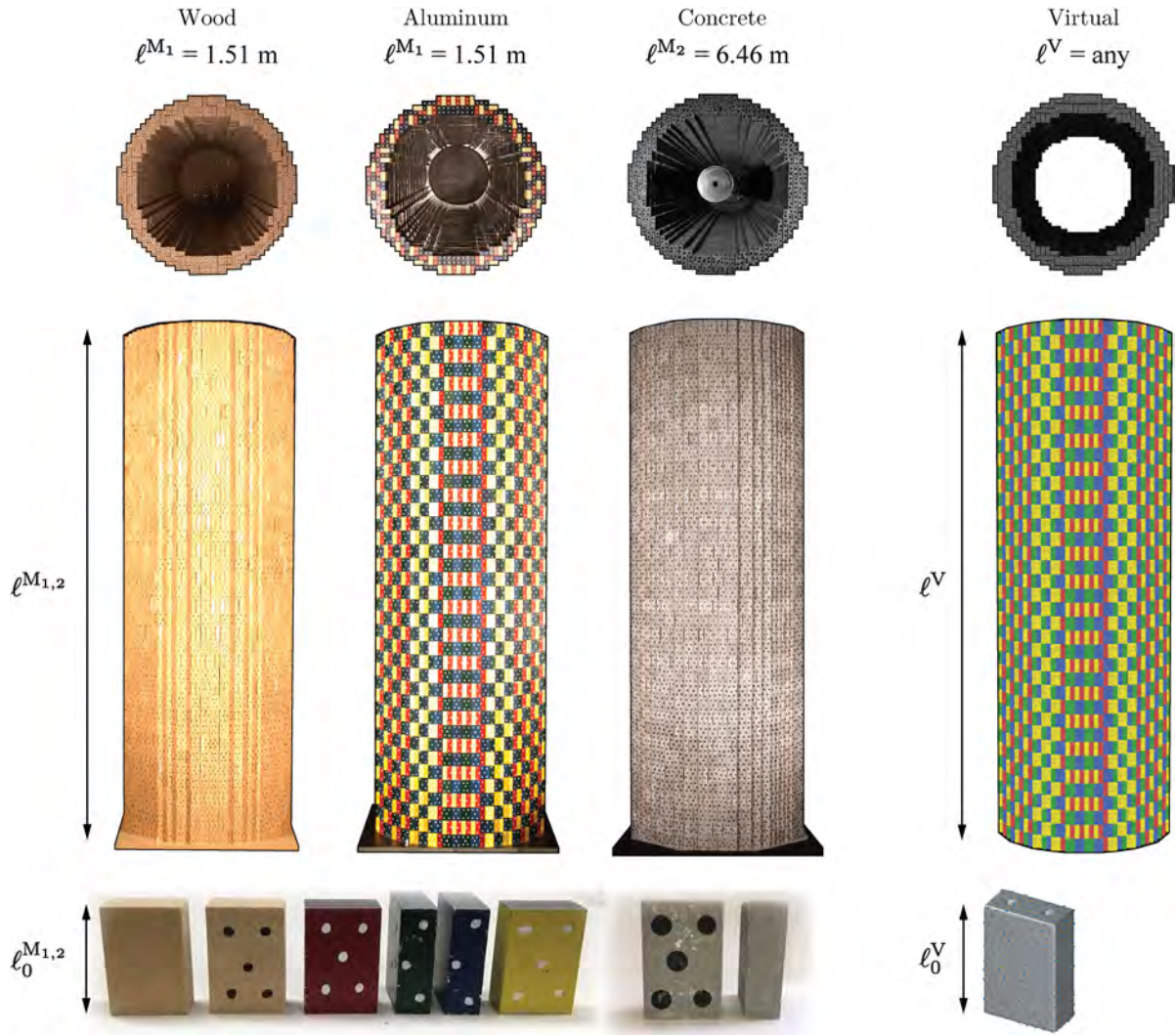
FIGURE 1 Model towers were built at two length scales with the same design for each. For the smaller length scale, M_1, towers were made of either wood or aluminum and at the larger length scale, M_2, all towers were made of concrete. Colors and dots were painted on blocks to improve the conducted digital image correlation (DIC). The pattern of the block arrangement as shown in the top view is rotated 90 degrees every layer and has symmetry such that every other layer is the same. The virtual tower is composed of blocks of identical size defined in shape by level set functions.

made of wood, aluminum and concrete materials experiencing both Ridgecrest and Denali ground motions for a total of six validation comparisons.

3 | MODELING METHOD

LS-DEM uses discrete level set functions to describe the shape of each object in a physical system.[17] In this paper, the objects of this system will be the blocks of the tower. A level set function, $\phi(\mathbf{x})$, will describe the block shape. The level set implicitly defines the block by outputting the signed distance, d, between a block's surface and an input location, $\mathbf{x}$.

$$\phi(\mathbf{x}) = \pm d \tag{5}$$

A negative distance indicates the input location is inside the block and a positive distance indicates that it is outside. The surface can always be determined from the zero level set. Because the blocks are built to be identical, only one level set definition is used for all blocks.
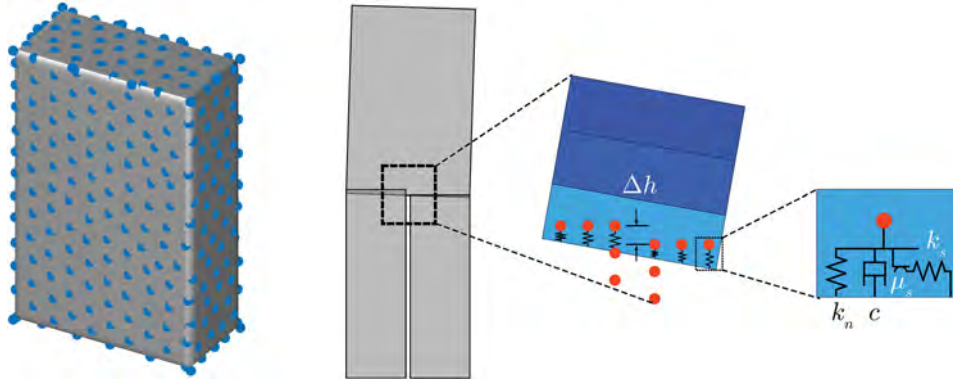
FIGURE 2 Visualization of a block's level set surface and surface points. Surface points are initially set to be equidistant then additional points are added at the corners and edges. Block height variation is a key aspect of the model, and therefore is shown in the sketch. The contact model uses linear springs in the normal and shear direction with a linear viscous damper in the normal direction and a Coulomb friction condition on the shear springs. Dimensional aspects are exaggerated in the figure for clarity.

TABLE 2 Discretization details for the LS-DEM model.

Parameter	Units	Value
Surface point density	$points/voxel^2$	0.05
Total surface points	$points$	440
Surface points on top surface	$points$	44
Voxel resolution for $\lambda = 1/107$	$mm/voxel$	0.65
Voxel resolution for $\lambda = 1/25$	$mm/voxel$	2.8

These level sets are used in conjunction with a set of discrete points with locations p_i placed on the surface of the blocks to determine contact. Each object has both a set of surface points and a level set function to serve as a leader and follower in the contact algorithm, respectively. Figure 2 visualizes both the level set surface and surface points for the block design. Details on the discretization are shown in Table 2. Discretization density and voxel dimensions were chosen to be similar to previous studies using LS-DEM in three dimensions. Surface points are randomly placed and equidistant from each other, then some additional surface points were added on the corners and edges to ensure sharp features.

When determining contact, the leader block will send the location of all of its surface points as input to the follower block's level set in a loop. The level set's output, the signed distances of the leader surface points to the follower's surface, determine if contact is established. Contact is determined to have occurred only if the level set function's output is less than zero for any surface point. For surface-to-surface contact, many surface points may satisfy this condition and all of them will contribute to the contact forces between the blocks. The distance result (if negative) is considered the penetration distance, and is multiplied by the blocks' normal stiffness, k_n, and surface normal, $\hat{\mathbf{n}}$, to determine the undamped normal force of the contact. A damping force is then applied to simulate the coefficient of restitution, C_{res}^N, of the contact. The addition of the undamped normal force and the damping produces the normal force for that contact point, F_n,

$$\text{if } \phi(\mathbf{p}_i) < 0 : \quad \mathbf{F}_n = \phi_j(\mathbf{p}_i)k_n\hat{\mathbf{n}} + \gamma_N(C_{res}^N)(\mathbf{v}^{rel} \cdot \hat{\mathbf{n}})\hat{\mathbf{n}} \tag{6}$$

where $\mathbf{p}_i$ is the set of locations of the surface points for the leader block, ϕ_j is the level set of the follower block, and $\mathbf{v}^{rel}$ is the relative velocity of the two contacting surfaces. The surface normal, $\hat{\mathbf{n}}$, is defined as the normalized gradient of the level set at the surface point location. The damping function, $\gamma_N(C_{res}^N)$, converts the coefficient of restitution to a corresponding fraction of the critical damping for the spring-damper system of that contact. The formula and derivation of the damping function is described in Harmon et al.[12] which contains a lengthy discussion of damping in LS-DEM.

The shear force is calculated from the relative velocity of the contact points on each block. Unlike the normal forces, the shear forces, F_s, are calculated using an incremental approach due to history dependence.

$$\Delta\mathbf{F}_s = k_s v_s \Delta t \,\hat{\mathbf{s}} \tag{7}$$

TABLE 3 Physical parameters for the LS-DEM model. The contact stiffnesses are more specifically the contact between particles not between points, therefore the point-to-level set stiffness is lower. The contact stress/displacement stiffness is the force/displacement stiffness divided by the top/bottom surface area.

Parameter	Units	Wood	Al	Concrete
Density (ρ)	kg/m^3	800	2632	2320
Normal stiffness (k_n)	MN/m	30	51	1050
	GPa/m	90	150	170
Shear stiffness (k_s)	MN/m	26	48	1000
	GPa/m	78	140	160
Friction coefficient (μ)	-	0.63	0.18	0.59
Coefficient of restitution (C_{res}^N)	-	0.3	0.5	0.5
Height variation (σ_H)	mm	0.16	≈ 0	0.5
Measured average block Height ($\bar{H}$)	mm	39.78	39.67	170.53
Coefficient of variance ($\sigma_H/\bar{H}$)	-	0.0040	≈ 0	0.0029

where k_s is the shear stiffness, v_s is the relative velocity of the contact points in the shear direction, Δt is the time step used to integrate (explicitly) the equations of motion, and $\hat{s}$ is the unit vector in the shear direction. The shear force increment is then normalized by the number of surface points in contact so that the shear force calculation is not discretization dependent. When the shear force builds to a critical value, the blocks are allowed to slip by the use of Coulomb friction

$$F_s^{max} = \mu F_n \tag{8}$$

Once both the normal and shear forces are determined the moments are calculated from crossing the center of mass, x_{cm} with the contact forces.

$$\mathbf{M} = \mathbf{x}_{cm} \times \mathbf{F} \tag{9}$$

Forces from the ground to the base layer of the tower are calculated from the surface points of the blocks. If any surface point from a block passes through the ground, then the penetration is calculated from the projection of the surface point to the plane that defines the ground. The shear forces are calculated similarly to block–block contact as well, where the relative velocity between a block and the ground is used to determine the shear force increment.

From the calculated forces and moments, the kinematics are then calculated using Newton's laws and an explicit time integration scheme with a consistent time step.[14] Damping the angular and translational velocities directly are a common technique in LS-DEM, often referred to as global damping.[12,17,28] This type of damping is not used in this model since global damping is generally meant for maintaining quasi-static conditions, whereas here the testing is dynamic in nature. The time the computations on the towers generally took were in the range of 3–5 h depending on the length of the ground motion and the material properties. The computations were done on an Intel Xeon CPU at 2.30 GHz with 18 cores/36 threads and 32 GB of RAM.

Blocks in experiment that are not made with precise enough dimensions affect the motion due to the heights being uneven. Uneven heights result in blocks initializing at an angle with their weight becoming unevenly distributed. In order to model this efficiently, the surface point locations at the top of each block were adjusted according to a normal probability distribution of height tolerance. The block arrangement is such that the block using surface points for contact is always under the block using the discrete level set function, and therefore if the surface points are adjusted for height the level set does not require adjustment. The physical properties were adjusted to account for the volume difference and the shift in center of mass.

4 | PARAMETER DETERMINATION

Every parameter in the model is determined through tests performed on individual blocks. The full list of parameters is shown in Table 3. Each part in this section will describe how to determine each parameter in the table. Due to both the
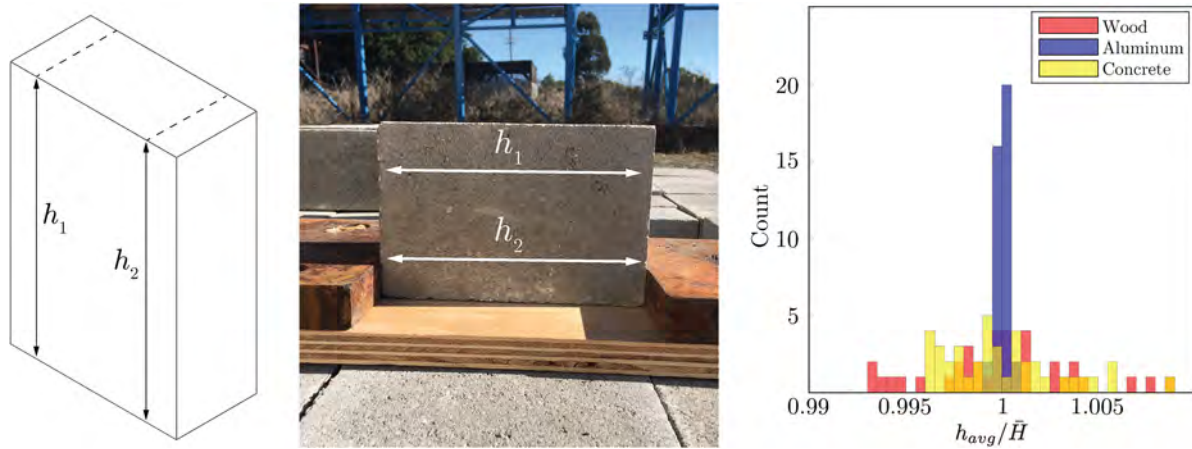
FIGURE 3 Block height is a key parameter in tower construction quality and dynamic response. Wooden blocks exhibit the greatest coefficient of variation ($=\sigma_H/\bar{H}$), followed by concrete, and then aluminum, which is a negligible amount.

rotations in the tower being very small and the low sensitivity of the model to the parameter, the section on the coefficient of restitution can be found in the appendix.

4.1 | Mass, volume, density and height variation

Geometry and mass are evaluated with digital caliper and scale measurements. The height of each block is determined as the average, $H = h_{avg}$, of measurements h_1 and h_2 taken at a distance roughly equal to a quarter of the width from each lateral edge, as shown in Figure 3. Note the quantity H is the measured height while the previously used parameter, ℓ_0, is the block height length scale parameter that is the target value for H. From a sample size of 40 blocks, the standard deviation of the block height for the aluminum, wood and concrete blocks are ≈ 0, 0.16 and 0.50 mm, respectively. The measured variance is a direct result of the manufacturing methods for each of the block types; carpentry for wood, CNC for aluminum, and machine pressed concrete blocks using a steel template. The height variation is a key parameter in the tower build quality and the dynamic response. The mass was measured for a sample of 10 blocks per type, yielding the densities reported in Table 3.
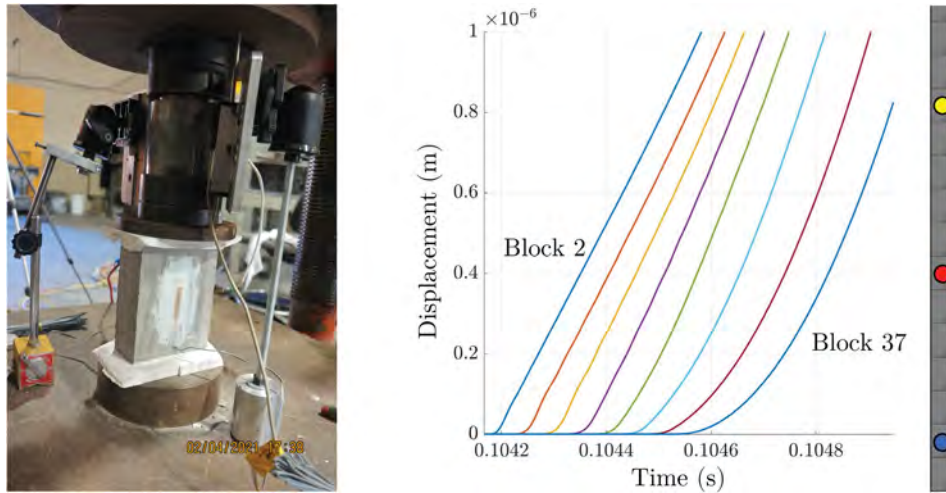
4.2 | Stiffness

When a stack of blocks are sitting on a moving surface, the blocks accelerate to meet the motion of the surface through the contact forces at the interfaces. In reality, these contact forces induce internal stresses that travel from the bottom to the top interface of a block at the material's wave speed. In the DEM, the time evolution of the internal stresses is not calculated, and instead the interfacial elasticity serves as a proxy. Therefore, the normal and shear stiffnesses are determined from the wave speeds of the material. In order to properly set the stiffnesses, we must first determine the material's wave speeds and then ensure that the stiffnesses are communicating motion at the same speed.

First, the aluminum wave speeds were determined with pressure and shear transducers placed on the block in pulse-echo mode. The distance traveled and the time delay from the pulse-echo directly yield the material wave speeds. This technique was insufficient for pressed wood and concrete as these materials disperse the signal and no clear measurement is possible. Compression tests were conducted on wood and concrete blocks to determine the Young's modulus and the shear modulus (ex. Figure 4). The bar wave speeds are then calculated as,

$$c_p = \sqrt{E/\rho} \tag{10}$$

for pressure waves and

$$c_s = \sqrt{G/\rho} \tag{11}$$

FIGURE 4 The block normal and shear stiffness are determined by matching the dilatational and shear wave speeds respectively to an effective material wave speed. The effective material wave speed is defined by the speed of transmitting stresses without sliding or rocking. The wave speeds for wood and concrete materials were determined from elastic moduli and density measurements while for aluminum the wave speed was determined directly.

for shear waves. We then adopted the idea of an effective wave speed which we define as the speed at which motion from the first layer propagates to the top of the tower in the DEM. We assume that the effective wave speed must equal the material wave speed for the tower motion to be properly predicted. The effective wave speed for the MTS can be measured in the DEM by simulating the motion of a one block per layer stack that is 38 layers tall. Each block in the stack was initialized just outside of contact then allowed to fall by gravity into place before receiving a ground motion. This is to ensure that the stack is in static equilibrium before a ground motion is applied. For determining the normal stiffness, this ground motion is in the vertical direction and for the shear stiffness the ground motion is in the horizontal direction. For both, the ground motion is applied in one direction only. In addition, the ability for the blocks to rotate or slide is disabled so only the translational motion resulting from the spring forces are measured.

The chosen ground motion was a unit step velocity at 80% the block height per second. This quick motion enabled easy identification of movement beyond the noise of any spring oscillations. The plot in Figure 4 shows the displacement of every fifth block over time for this ground motion. The effective wave speed can be measured in this plot from the difference in time it takes blocks a certain distance apart to reach the same displacement.

4.3 | Friction coefficient

The static friction coefficient is determined by measuring the angle when slip initiates. This critical angle is measured using a wedge plate for both block–block interfaces and base–block interfaces to assure that the system can be characterized by a single friction coefficient for each of the three materials tested. Figure 5 shows the experimental setup for the static friction testing of concrete. To keep the blocks from rocking over, the center of mass of the top of the block was lowered by attaching some weight to it. Care was taken for the concrete tests that the side that was open to the mold was not used. The results are reported in Table 3 and can also be seen in Figure 5.

5 | SPECIMEN PREPARATION

In order to properly study the effect of a ground motion on a tower, the tower must first settle into a configuration that is in a state of stable static equilibrium. This task is trivial for towers where every block has the same height since the blocks can be placed surface-to-surface. Initializing the location of every block just out of contact in its designed location and allowing them to reach equilibrium via gravity is sufficient for a well assembled tower. When blocks vary in height however, this strategy is insufficient. The height discrepancies create non-flat surfaces for blocks to rest on since all blocks above the
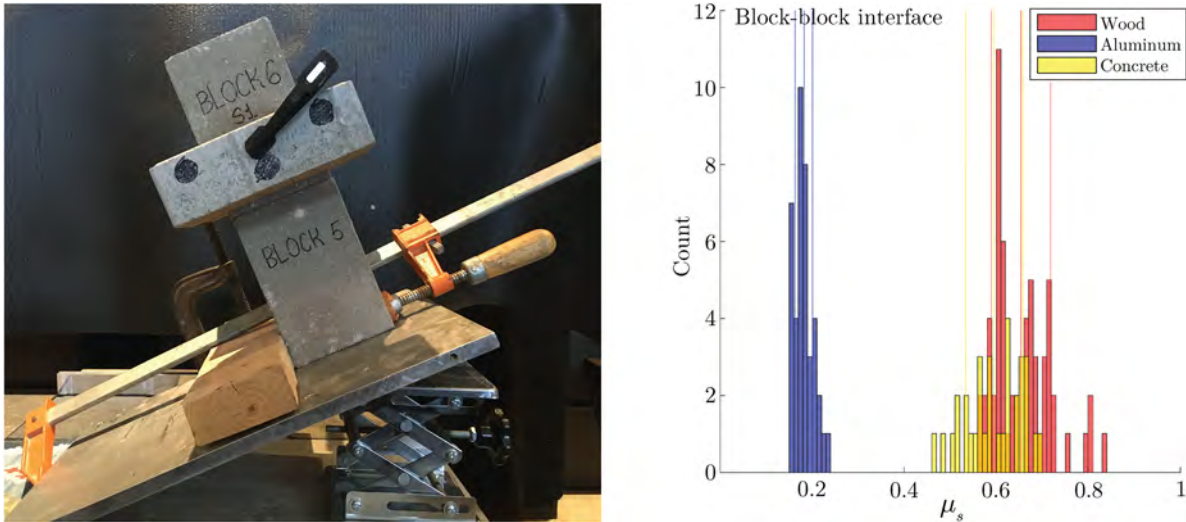
FIGURE 5 Static friction test conducted on block-block and block-base interfaces. The wedge angle is slowly increased until slip initiates. A histogram of block–block interface measurements shows that wood and concrete have roughly the same friction coefficient.

first layer are situated over exactly two blocks of different height below. In order to find equilibrium, blocks must rotate to engage both contact surfaces. The kinetic energy from this extra rotation will cause excess motion from both the top block that is rotating and the blocks underneath which results in a damaged tower before experiencing any ground motion. For MTS, we define damage as block misalignment, at no point is there any study into damage of the block material and it is assumed that there is little to no material damage until final collapse. In experiments, the towers are constructed one block at a time, but one at a time stacking would take unreasonable computational time in the numerical model. Instead, the tower is assembled layer-by-layer which also has a drawback. Layer-by-layer assembly introduces an unacceptable amount of kinetic energy into the tower even when bricks are initiated immediately above their equilibrium location. To overcome this, the block velocities are damped to ensure reasonable kinetic energies throughout the preparation process. This damping strategy is separate from the damping produced by the coefficient of restitution, and is only used for the preparation phase to specifically resemble the motion of a block being placed by hand into place in a tower. For the ground motions, this damping is not used.

Damping is applied by multiplying each block's velocity by a constant, c_v, every time step

$$v_{damped} = (1 - c_v) v \tag{12}$$

Very little damping is needed to achieve stable towers, and so damping values $c_v \leq 0.002$ were used throughout. New layers only are added after the previous have settled. This process significantly limits the initial damage compared to dropping all the layers at once.

For this initialization work, the blocks were enlarged by the maximum expected contact overlap during specimen preparation so when the prepared tower is initialized for a ground motion test, the blocks start out of contact. This way, new parameters could be tested for the same specimen without having to redo the preparation phase. Otherwise, the initial overlaps would not be in equilibrium with new parameters and therefore cause immediate instability. Because of this, a short initial phase of zero ground motion was added before each test to allow the prepared specimen to re-establish static equilibrium under gravity.

The key difference for towers with block height variability is that many blocks will begin with a non-zero rotation, reducing the required rotation to reach the critical point where rocking would occur. Note that the critical overturn angles for a single block of these dimensions are 17.7° for the thin side and 33.6° for the wide side. Figure 6 visualizes the initial rotations of the blocks in the numerical tower. As shown in Table 3, the block height variability is significantly different for each material due to the different methods of fabrication. Increasing variability in block height leads to increasing initial rotation. Aluminum blocks have very little initial rotation while some wood blocks initialize with rotations > 5°. We assume that the ground surface is perfectly flat so the first row of blocks always start with an initial rotation of zero.
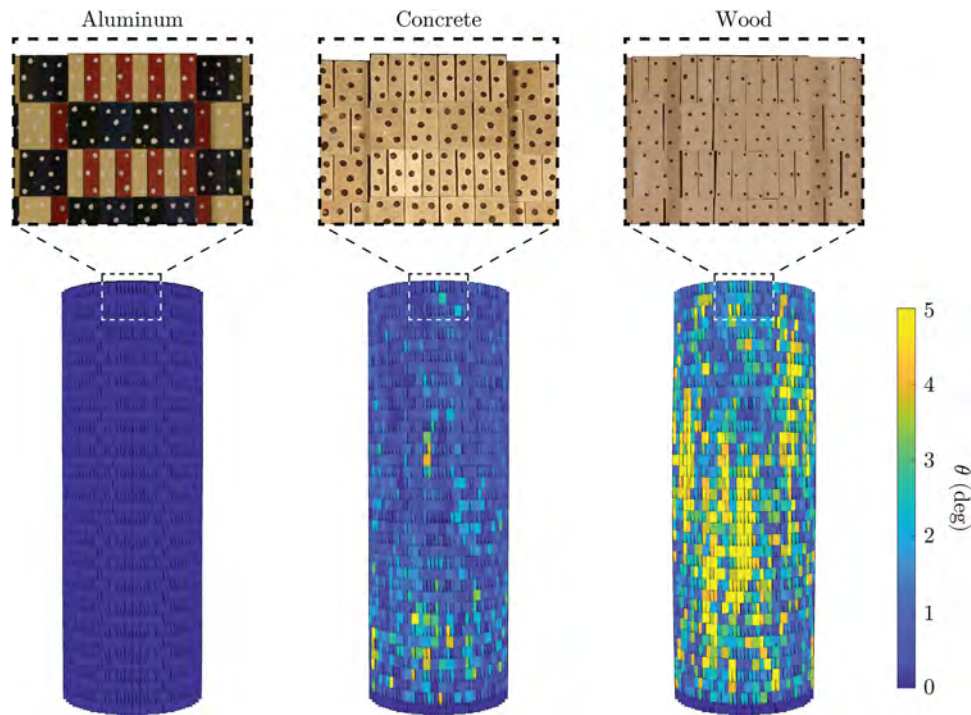
FIGURE 6 Visualization of initial block rotations after numerical tower specimen preparation and before ground motion. Progressively increasing height variability increases initial damage. Damage for MTS is defined as block misalignment, for which initial rotations are a good indicator. Above each tower is a section image of the corresponding experimental specimen the numerical tower is attempting to recreate.

TABLE 4 Simulation time steps and DIC camera frame rates.

Parameter	Units	Wood	Aluminum	Concrete
Time step	μs	10.4	2.6	14.7
Camera frame rate	*fps*	4800	4800	2000

6 | RESULTS

The goal of this section is to demonstrate the predictive capabilities of LS-DEM on MTS and to show the effect of friction and block height variability on the dynamics of the blocks. The validation portion will be done through two synergistic methods of comparison. First, we will compare the visualization of the computation to digital image correlations (DIC) on the experimental images. In order to minimize differences in methodology, DIC was conducted on the visualization of the virtual model as well, with the virtual camera placed at the same location as the camera in the experiments. This method accounts for possible inaccuracies in measurements at the top and bottom of the tower that arise due to the viewing angle of the camera. DIC on both the experimental and virtual images were conducted at 4k resolution. Simulations were conducted using a constant timestep that is a factor of the camera's framerate to ensure that visual comparisons occur at exactly the same time, these values are shown in Table 4. The DIC comparisons were completed for the full video of each test and here three representative time steps will be shown for the wood tower experiencing one-component Ridgecrest and the concrete tower experiencing three-component Ridgecrest as examples in Figure 7. In the figure, the velocity in the in-plane horizontal direction is shown in color as the basis for comparison. The matches between the experimental measurement and the corresponding LS-DEM predictions is remarkable, and are of similar quality for towers not shown here due to space limitations.

The second method of comparison will be comparing the velocities of a set of blocks over time. For the virtual model, the centroid of the block will be used and for the experiment the center of the front face measured from DIC will be used. The set of blocks chosen are shown in Figure 7 as dots on the towers and will be referred to as the "spine" of the tower. Each block of the set is in the same location in the tiling pattern and two layers above each previous block. Due to the MTS having a two-layer block pattern repetition, the neighborhood of each spine block has an identical orientation. The
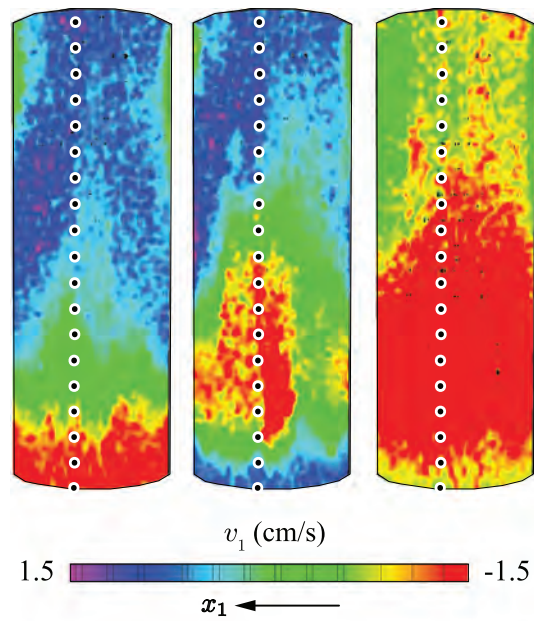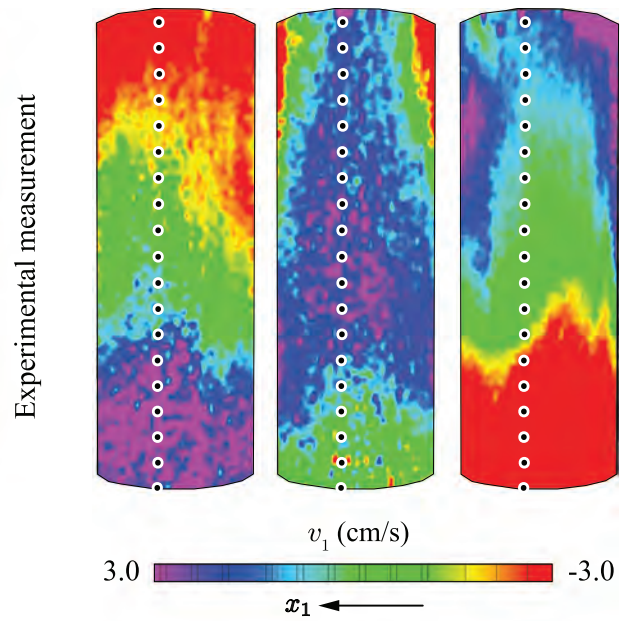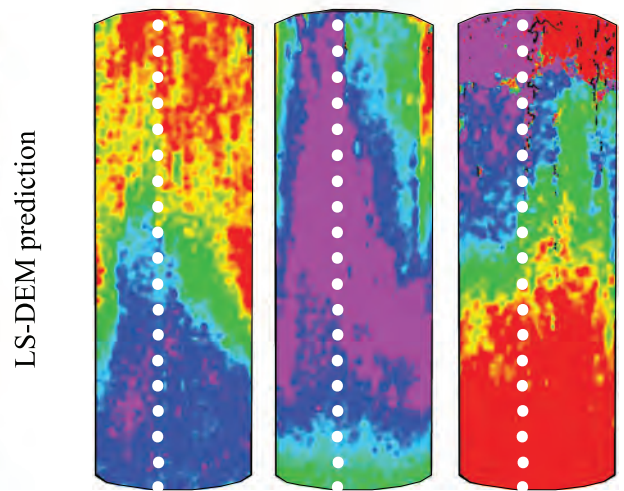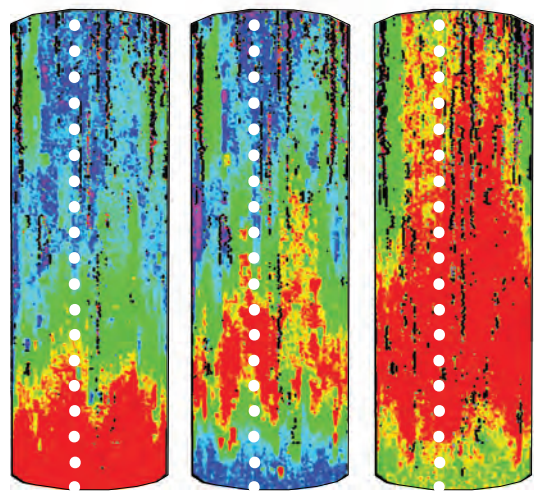
a) Ridgecrest 1D: v_1 field, $\lambda_\ell = 1/107$

b) Ridgecrest 3D: v_1 field, $\lambda_\ell = 1/25$

$t_1 = 0.71650$ s $t_2 = 0.73520$ s $t_3 = 1.00400$ s

$t_1 = 3.1240$ s $t_2 = 3.2320$ s $t_3 = 3.8095$ s

FIGURE 7 A sample of the DIC comparisons conducted between experiment and the numerical model. The left side shows wood towers at $\lambda_\ell = 1/107$ that experience a single component ground motion. The right side are concrete towers at $\lambda_\ell = 1/25$ that experience a three-component ground motion.

spine allows the quantitative comparison of important dynamic features such as the amplitude of motion and structural speed. The structural speed is defined as the speed at which motion travels from the bottom of the tower to the top. This is similar to effective wave speed except that now the effects of sliding, rotation and block height variation slow the speed down significantly.

Figure 8 shows this comparison for six distinct experiments. Since the numerical tower models use a probability distribution to generate the random block heights, many comparisons here show the average value and standard deviation of the spine velocities taken from ten realizations of block heights. Note that the mean value of 10 velocity response time histories introduces some smoothing of the velocity profile compared to the experimental results which do not contain this smoothing effect. This was not done for the aluminum towers, however, since the height variation was negligible for aluminum blocks. The six spine comparisons span two ground motions, two scales and three materials. As shown in
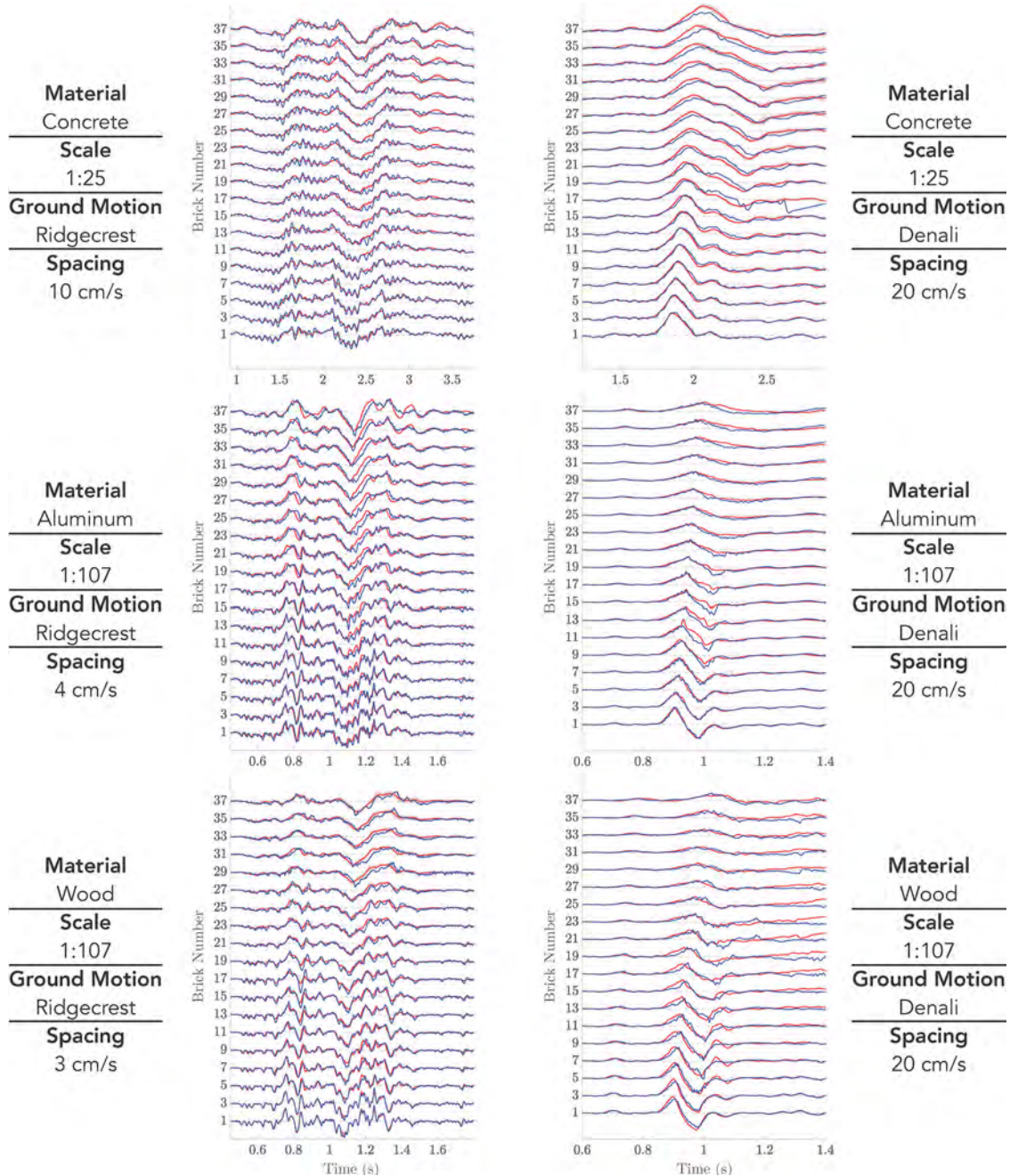
FIGURE 8 Each plot shows the velocity of a block on every other floor both from the experiment (blue) and from the centroid motion in the numerical model (red). The red line and shaded area over it indicate the mean and mean +/- standard deviation interval of the velocity time histories obtained from 10 random realizations of the tower block heights (obtained from 10 specified distinct seed numbers) for that material. Spacing is the y-axis separation between each plot in velocity.

Table 3, the chosen materials span a significant range of mass densities, friction, and height variability, demonstrating the predictability of the model over significant ranges of values of key parameters of the tower.

The DIC comparisons focused on validating the kinematics of the entire MTS at single time steps and the spine comparisons focused on validating the kinematics of single locations over the entire time history. Together these methods of comparison provide a synergistically comprehensive method of validation.

For all towers that were constructed, ground motions were applied until failure (caused by either a ground motion applied once or the same ground motion applied multiple times sequentially). Only complete failures were observed; for no tower did only a portion of the tower fall before the rest of the tower. For all cases, the tower survived the first

application of the Ridgecrest motion, even for the concrete tower when all three components of the ground motion were applied. In fact, the wood and aluminum towers survived four successive uni-axial Ridgecrest ground motions, though with damage accumulation after each.

Damage can be evaluated through the permanent displacement and rotation of blocks in the tower. Example damage data is shown in Figure 10 where the displacements, slip and x_3-axis rotations are shown for the wood tower spine experiencing Ridgecrest. For the wood tower, slip was minimal, but the rotations were significant. Vertical axis rotations were key to understanding the damage level in all towers. The experimental techniques used here were unable to measure the x_3-axis rotations for anything other than the top floor, highlighting the importance of modeling for this and future studies on MTS.

After surviving all four, the damaged towers were subjected to the Denali ground motion to ensure collapse. The concrete tower fell on the third three-component Ridgecrest motion experienced, and so never experienced a Denali ground motion from an initial damaged state. All towers fell when experiencing uni-axial or tri-axial Denali, regardless of scale, material or damage. An interesting observation made and shown in detail in the experimental papers of the research campaign is that initial damage does not affect the dynamic response behavior of the towers.[26,27] This was discovered by observing little difference in the DIC and the spine plots for successive Ridgecrest motions applied to the same tower. The major difference between damaged and undamaged towers at a local scale is that contact surface areas between blocks reduce with damage. Because friction force is independent of contact surface area, it is sensible that any amount of misalignment before toppling would produce the same tower motion.

Both experiment and simulation showed the same failure modes given the same conditions. Two distinct failure modes were observed over all the tower specimens tested. Figure 9 shows each, which will be called a "buckling" and "peeling" mode. The buckling mode occurred only for the towers with higher friction coefficients, specifically the wood and concrete towers subjected to the Denali ground motion. This buckling mode is characterized by a bulging outward in the middle section of the tower causing a mostly downward but also slightly inward collapse for the blocks above the bulge. Once the buckle matures, the rest of the tower quickly accelerates to failure where the unbuckled sections are pushed outward from the top by the inward collapsing blocks. The peeling mode was observed from the concrete Ridgecrest collapse and the aluminum Denali collapse. This failure mode initiates from a section of blocks rocking outward together, usually initiating near the center. This peeling mode collapses the rest of the tower from a domino-like effect caused by the interlocking of the tiling design. The result of this is that nearly the whole tower fails outward.

6.1 | Friction effect

The presence of friction both transfers energy through the system but also dissipates energy if sliding occurs. By varying the friction coefficient the critical point at which sliding is initiated changes. If the ground motion acceleration is low enough for sliding to not initiate for the range of friction coefficients tested, then no change in the tower dynamic response behavior should be detected. However, if the ground motion acceleration is high enough, there will be a difference in the tower response. In order to test the effects of the friction coefficient value, four numerical wood towers with no block height variability were produced, each with different friction coefficients. No block height variation was used so the initial conditions could be consistent for each tower. All four towers were subjected to the same uni-axial Ridgecrest ground motion used previously for the wood towers. In Figure 11 the velocity of uppermost block on the spine is shown for friction coefficients varying from $\mu = 0.1$ to $\mu = 0.63$. Only the highest layer is shown since this is where the differences are most severe.

It can be immediately observed that the motion of layers with lower friction exhibit a lag in velocity changes, a direct effect of less shear force being possible. In the early stages of the motion, this serves to reduce the amplitude of shaking such as near $t = 0.8$ s. At later stages when the blocks reach higher velocities however, the lower friction blocks cannot slow down as quickly such as near $t = 1.4$ s. For all values of friction, the structural speed can be observed by the alignment of the peaks and troughs of the velocities in time. If they are aligned, then the structural speed between the towers at this time is the same, since the motion reached the top layer at the same time. However, if they are not aligned, then there is a difference in structural speed. By such observations, the structural speed is only affected at the later part of the motion when significant sliding is evident from the amplitude differences. Such an observation is expected since sliding must initiate for friction to affect the structural speed. So while blocks are still in the stick mode, such as near $t = 0.75$ s, the structural speed should be the same regardless of friction. Because dynamic response is independent of damage, if at intermediate times the ground motion acceleration is
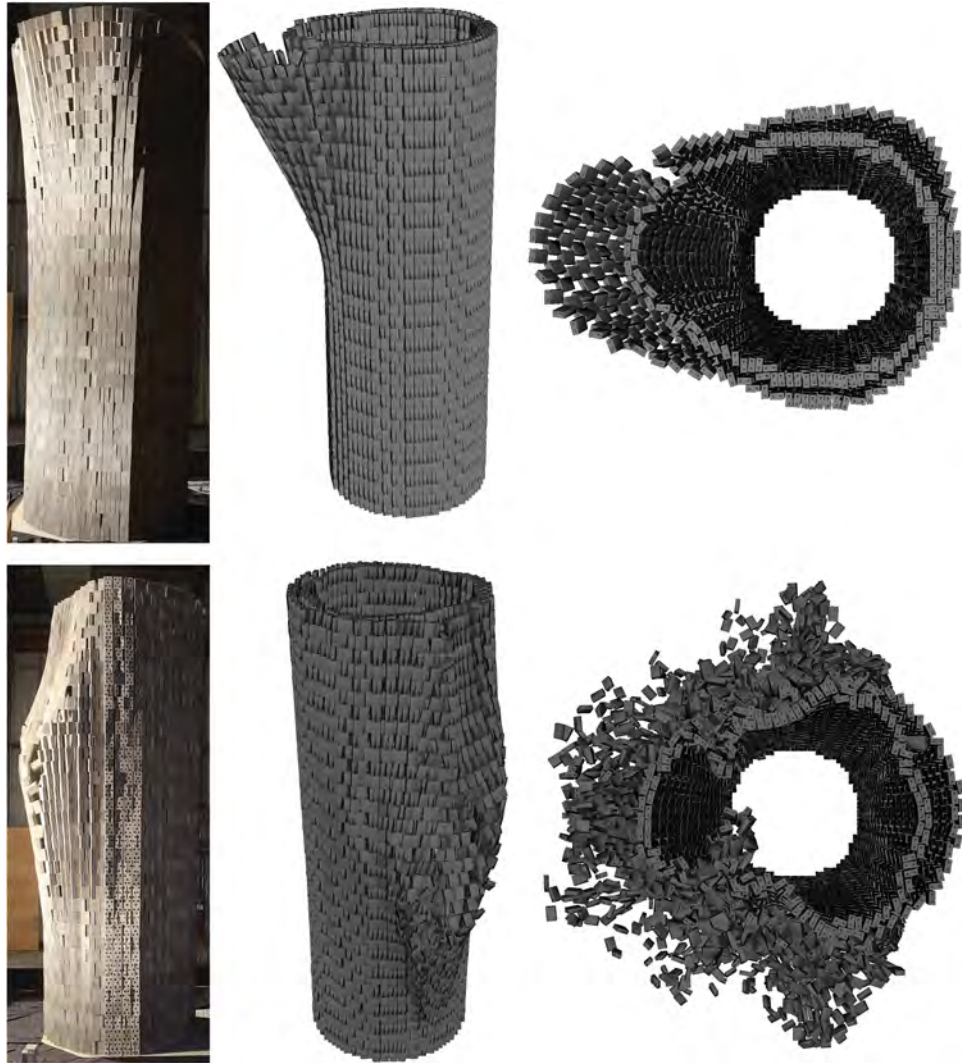
FIGURE 9 Most towers failed by a "peeling" mode (top). The wood and concrete towers that experienced Denali, however, failed with an observable buckle in the mid section of the tower (bottom). The experiment (left) and the numerical model (right) agreed on the failure mode for all tests.

low enough for blocks in the low friction tower to stop slipping, then it will return to the same behavior as the high friction towers.

6.2 | Block height variability effect

By varying the height of the blocks, the contact surfaces between layers are no longer flat and consistent. This results in blocks initializing at an angle and therefore being more susceptible to rocking. This also affects the friction since block misalignment will cause an uneven distribution of force on lower layer blocks. Figure 12 compares the dynamics of the numerical wood tower experiencing the Ridgecrest ground motion both with and without random block height variability.

Block height variability does not seem to significantly affect the amplitude of the velocity response. This effect is easily observed by the velocity peaks being of similar values. However, block height variability has large effects on the structural speed. Peaks in velocity near $t = 0.8$ s and $t = 1.1$ s clearly occur much later for the towers with height variability. This effect is well beyond one standard deviation of velocity from the 10 random realizations of the tower block heights. The vertical force chains in the towers with variable block heights are no longer completely vertical, requiring forces to be communicated along a farther distance, slowing down the structural speed.
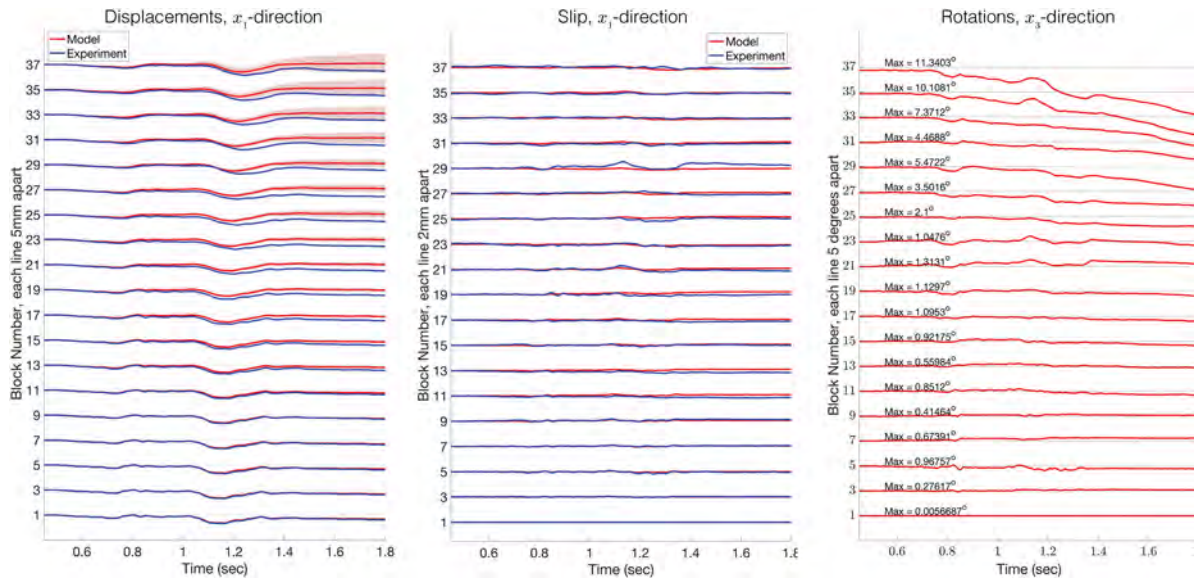
FIGURE 10 Tower damage is best evaluated by permanent kinematic motion, three aspects of which are shown in this figure for the wood tower experiencing Ridgecrest. Left) Displacements of the blocks along the spine for model and experiment with shading for the standard deviation of 10 towers with different height variation seeds. Middle) Slip is calculated by the difference in displacement between floors. Little slip is found for this example since wood has high friction. Right) Rotations around the vertical axis are a consistently observable marker for damage for all types of towers.
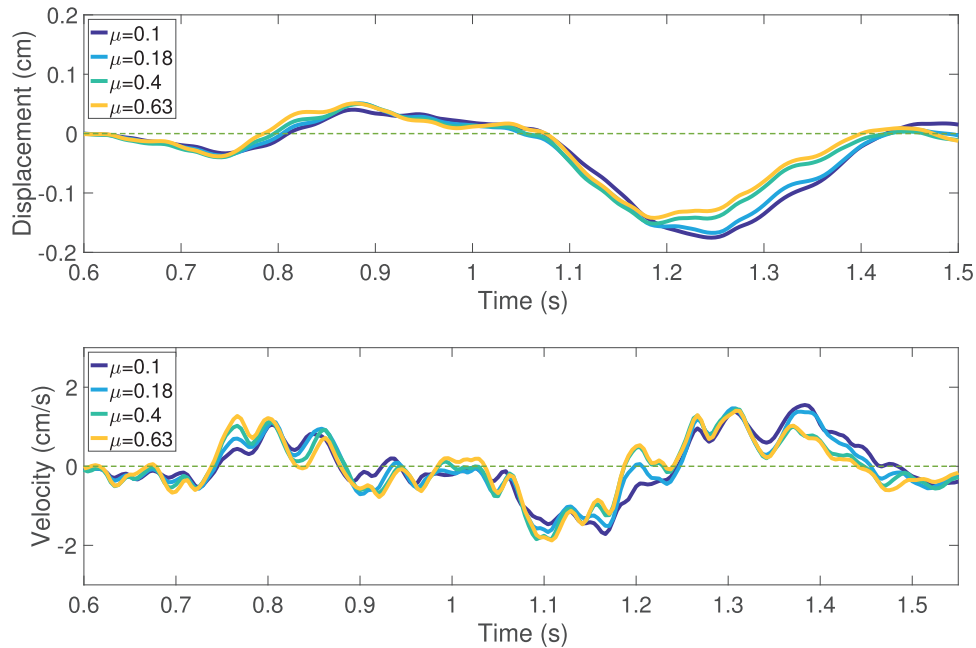
FIGURE 11 Velocity of a single block on the 37th layer of the numerical tower with varying friction coefficients. For each test, the friction coefficient is the same for all the blocks in the tower. Changes in friction significantly affects the velocity amplitudes. Structural speed is also affected, but for this ground motion, sliding does not occur for long enough cumulative time for this to be a pronounced effect.

It is not obvious from Figure 12 that block height variability actually impairs stability, however towers that have block height variability do collapse easier. This comes from blocks initiating with a non-zero angle and misalignments being closer to the critical point of failure than blocks of identical heights starting from near-perfect alignment.
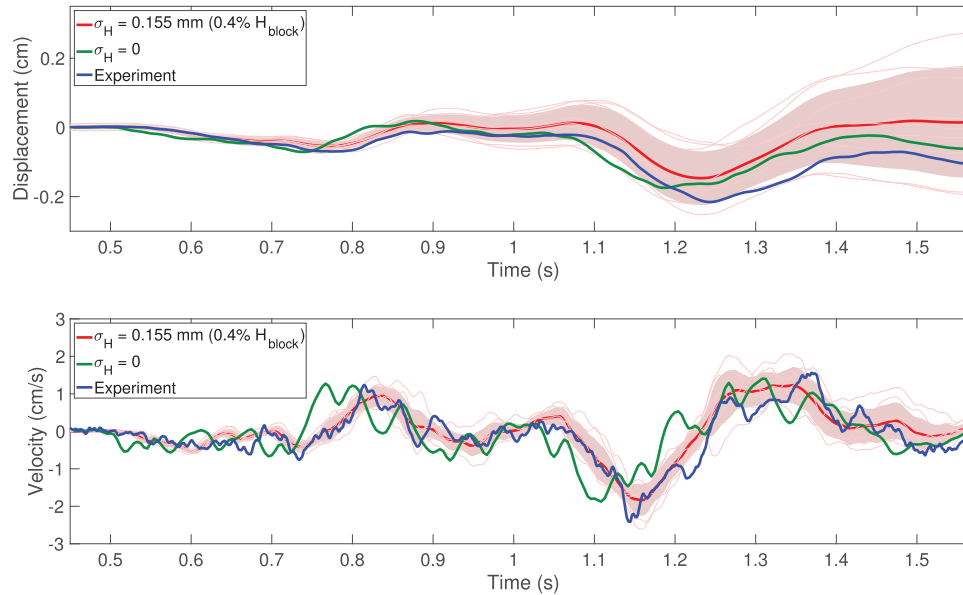
FIGURE 12 If the blocks are not all the same height then significant changes to the dynamics will take effect. This plot shows the velocity of the spine block on the 37th level for towers with and without consistent block height. A total of 10 towers with block height variability were modeled and the red line and shaded area over it indicate the mean and mean +/- standard deviation interval of the velocity time histories obtained from 10 random realizations of the tower block heights (obtained from 10 specified distinct seed numbers) for that material. The experiment is shown as well to demonstrate the improved prediction with block height variability. The thin red lines show the 10 individual realizations of the velocity response histories.

7 | CONCLUSION

MTS are promising new structures for the storage of gravitational energy which have been shown in this paper to be predictable with LS-DEM under seismic conditions. It was shown that the parameters for LS-DEM can be fully determined from small experiments and material measurements, all of which can be conducted from individual blocks before starting the construction of a tower. The predictability of LS-DEM was demonstrated for many scales, materials and ground motions, showing that the method correctly describes many of the features of the seismic response of MTS. The method can also predict failure modes, with two distinct modes observed, namely the "buckling" and "peeling" mode. These predictions allowed parametric studies showing that the friction coefficient affects the amplitudes of velocity of the blocks and the block height variability affects the structural speed.

Further work on MTS should focus on new tower designs, targeting increased stability and new failure modes. All the towers considered herein were constructed of the same block design, so future work should look into different block designs since the block height to base ratio has a well established effect on rocking.[29] Non-flat surfaces could increase interlocking and LS-DEM is uniquely capable of modeling these with concave features.

In terms of the MTS model, some improvements could be added to decrease the current discrepancies with experimental results. Adding the rotational components of earthquake ground motions would be important, since these structures are more susceptible to rocking than continuous structures. All blocks used in the model also had the same discretization. It is likely that a more refined discretization of the surface points would improve results. Finally, is it well known that rate-and-state friction models are an improvement over Coulomb friction, so their addition to this model could be worth the additional complexity.

DATA AVAILABILITY STATEMENT

The data that support the findings of this study are available from the corresponding author upon reasonable request.

ORCID

Joel P. Conte https://orcid.org/0000-0003-2068-7965
José E. Andrade https://orcid.org/0000-0003-3741-0364

REFERENCES

1. Markolf S, Azevedo I, Muro M, Victor D. Pledges and progress: steps toward greenhouse gas emissions reductions in the 100 largest cities across the United States. *Brookings Institute*. October 2020. brookings.edu
2. Loveless M. Energy storage: the key to a reliable, clean electricity supply. What is the potential impact? Energy.gov 2012. (Accessed 2021).
3. Water Power Technologies Office, Office of Energy Efficiency and Renewable Energy. Pumped Storage Hydropower. (Accessed 2021). energy.gov/eere/water/pumped-storage-hydropower
4. Marfia S, Sacco E. Multiscale damage contact-friction model for periodic masonry walls. *Comput Methods Appl Mech Eng*. 2012;205-208:189-203. Special Issue on Advances in Computational Methods in Contact Mechanics.
5. Sacco E, Toti J. Interface elements for the analysis of masonry structures. *Int J Comput Methods Eng*. 2010;11:354-373.
6. Petracca M, Pelà L, Rossi R, Oller S, Camata G, Spacone E. Multiscale computational first order homogenization of thick shells for the analysis of out-of-plane loaded masonry walls. *Comput Methods Appl Mech Eng*. 2017;315:273-301.
7. Brasile S, Casciaro R, Formica G. Multilevel approach for brick masonry walls – part I: A numerical strategy for the nonlinear analysis. *Comput Methods Appl Mech Eng*. 2007;196(49):4934-4951.
8. Pelà L, Cervera M, Roca P. Continuum damage model for orthotropic materials: Application to masonry. *Comput Methods Appl Mech Eng*. 2011;200(9):917-930.
9. Cundall PA, Strack ODL. A discrete numerical model for granular assemblies. *Géotechnique*. 1979;29(1):47-65.
10. Kawamoto R, Ando E, Viggiani G, Andrade JE. All you need is shape: predicting shear banding in sand with LS-DEM. *J Mech Phys Solids*. 2018;111:375-392. 2018.
11. Lisjak A, Grasselli G. A review of discrete modeling techniques for fracturing processes in discontinuous rock masses. *J Rock Mech Geotech Eng*. 2014;6(4):301-314.
12. Harmon JM, Karapiperis K, Li L, Moreland S, Andrade JE. Modeling connected granular media: particle bonding within the level set discrete element method. *Comput Methods Appl Mech Eng*. 2021;373(1):113486.
13. Guo Y, Morgan JK. Fault gouge evolution and its dependence on normal stress and rock strength: Results of discrete element simulations: Gouge zone micromechanics. *J Geophys Res*. 2008;113(B8).
14. Lim KW, Andrade JE. Granular element method for three-dimensional discrete element calculations. *Int J Numer Anal Methods*. 2014;38(2):167-188.
15. Mollon G, Zhao J. 3d generation of realistic granular samples based on random fields theory and Fourier shape descriptors. *Comput Methods Appl Mech Eng*. 2014;279:46-65.
16. Potapov A, Campbell C. A three-dimensional simulation of brittle solid fracture. *Int J Mod Phys C*. 1996;7:717-729.
17. Kawamoto R, Andò E, Viggiani G, Andrade JE. Level set discrete element method for three-dimensional computations with triaxial case study. *J Mech Phys Solids*. 2016;91:1-13.
18. Cheng YP, Nakata Y, Bolton MD. Discrete element simulation of crushable soil. *Géotechnique*. 2003;53(7):633-641.
19. Lemos JV. Discrete element modeling of the seismic behavior of masonry construction. *Buildings*. 2019;9(2):43.
20. Pulatsu B, Bretas EM, Lourenco PB. Discrete element modeling of masonry structures: validation and application. *Earthq Struct*. 2016;11(4):563-582.
21. Caliò I, Marletta M, Pantò B. A new discrete element model for the evaluation of the seismic behaviour of unreinforced masonry buildings. *Eng Struct*. 2012;40:327-338.
22. Sarhosis V, Baraldi D, Lemos JV, Milani G. Dynamic behaviour of ancient freestanding multi-drum and monolithic columns subjected to horizontal and vertical excitations. *Soil Dyn Earthq Eng*. 2019;120:39-57.
23. Komodromos P, Papaloizou L, Polycarpou P. Simulation of the response of ancient columns under harmonic and earthquake excitations. *Eng Struct*. 2008;30(8):2154-2164. Seismic reliability, analysis, and protection of historic buildings and heritage sites.
24. Andrade J, Rosakis AJ, Gabuchian V, et al. A framework to assess the seismic performance of multiblock tower structures as gravity energy storage systems. *J Eng Mech*. 2022.
25. Rosakis AJ, Andrade J, Gabuchian V, et al. Implications of Buckingham's Pi theorem to the study of similitude in discrete structures: introduction of the RFN, μN, and SN dimensionless numbers and the concept of structural speed. *J Appl Mech*. 2021;88(9):091008.
26. Gabuchian V, Rosakis AJ, Harmon JM, Andrade JE, Conte J, Restrepo J. Multiscale experiments for seismic performance assessment of multiblock tower structures for energy storage: 1/107 scale. *Submitted to Earthquake Engineering and Structural Dynamics*. 2022.
27. Restrepo J, Gabuchian V, Harmon J, et al. Multiscale experiments for seismic performance assessment of multiblock tower structures for energy storage: 1/25 scale. *Submitted to Earthquake Engineering and Structural Dynamics*. 2022.
28. Karapiperis K, Harmon J, Andò E, Viggiani G, Andrade JE. Investigating the incremental behavior of granular materials with the level-set discrete element method. *J Mech Phys Solids*. 2020;144:104103.
29. Housner GW. The behavior of inverted pendulum structures during earthquakes. *Bull Seismol Soc Am*. 1963;53(2):403-417.

30. Shenton III HW, Jones NP. Base excitation of rigid bodies. I: Formulation. *J Eng Mech*. 1991;117(10):2286-2306.
31. Gallego E, Fuentes J, Ruiz A, Rodrigo GHS, Aguado P, Ayuga F. Determination of mechanical properties for wood pellets used in DEM simulations. *Int Agrophys*. 2020;34:485:494.

APPENDIX: COEFFICIENT OF RESTITUTION

Within this study, very little rocking can occur before reaching collapse. Figure A1 shows that the rocking rotations at every level of the spine remains negligible throughout a ground motion. Due to minimal rocking rotations, the dissipation from rocking impact plays little part in the results. Despite this, a small study on rocking and the coefficient of restitution parameter for wood in LS-DEM was done.

The coefficient of restitution measures the elasticity of collisions. A value of zero indicates an inelastic collision where all the kinetic energy is absorbed, and a value of one indicates a perfectly elastic collision where no kinetic energy is lost. The coefficient of restitution is well understood for collisions with initial and final relative velocities along the same line of action as the surface normal of the contact surface. It is in this way that the coefficient of restitution, C_{res}^N, is implemented in LS-DEM. However, in the present case, the most important collisions happen when a block is rocking. A block rocking will collide with the surface it is rocking on often many times before coming to rest.
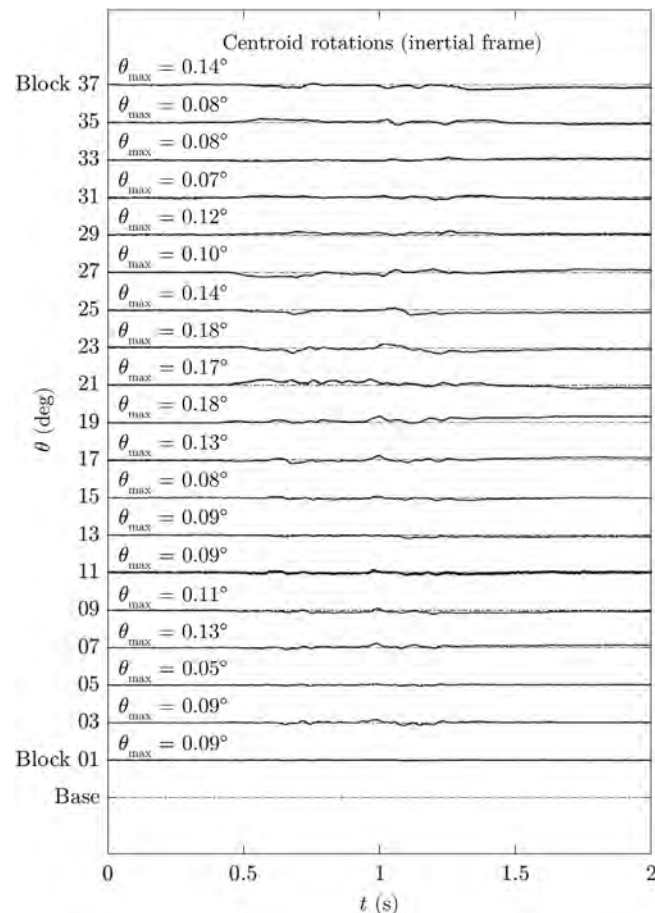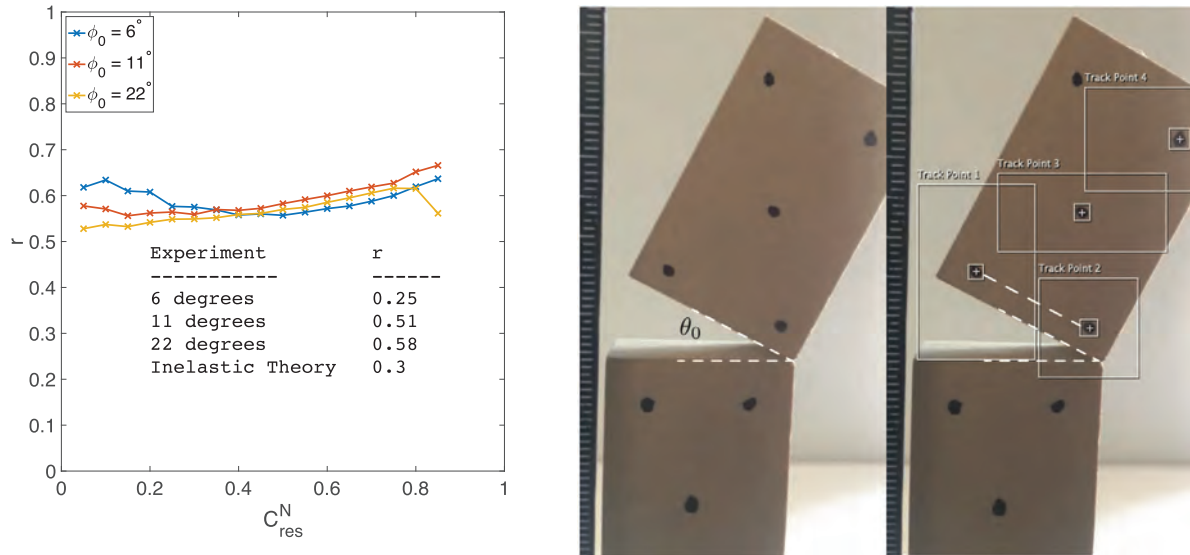

FIGURE A1 Rocking rotations along the spine with the maximum angle shown for the wood tower experiencing Ridgecrest. Rocking rotations for tower that did not collapse remained very small, minimizing the importance of rotational impacts on the tower kinematics.

FIGURE A2 (Left) Reduction of kinetic energy per collision during rocking motion, r, versus the coefficient of restitution, C_{res}^N, from the blocks in the model. The model predicts well the experiments at higher initial angles. (Right) Rocking test conducted on wood blocks. Motion tracking of markings yields the block angle that could be matched to the rotations predicted in simulation.

An important study on the theory of rocking was conducted by Housner.[29] This theory demonstrates that for an inelastic collision (no bouncing in the vertical direction), the moment of momentum about the rocking point is conserved and so the ratio of kinetic energy before impact to the kinetic energy after impact, r, can be determined by

$$r = \left[1 - \frac{mR^2}{I_0}(1 - \cos 2\alpha) \right]^2 \tag{A1}$$

where m is the mass of the block, R is the distance from the center of the block face to the corner, I_0 is the mass moment of inertia about the corner, and α is the angle between R and the block height. For blocks of all materials and scales in this study, r is predicted to be ≈ 0.3 from this theory if their collisions are indeed inelastic. This sets a lower bound for possible true values of r since some bouncing likely occurs.

In order to test rocking directly, wood blocks were held at a set angle and when released, allowed to rock until coming to rest. To confirm there is no slide rocking occurring during the test, we refer to the derivations of Shenton and Jones.[30] From this study, we know that slide-rocking occurs when the following inequality is broken,

$$\mu \geq \left| \frac{\frac{H}{B}(\lambda_x - C_{res}^N)}{1 + C_{res}^N} \right| \tag{A2}$$

where H and B are the height and width of the block, respectively, and λ_x is proportional to the lateral motion of the impact point which is zero in these experiments. Using this equation, we know for this case, there will be no slide rocking if the coefficient of restitution for the wood is below 0.67. While we have not seen a study for coefficient of restitution for the wood type we used, other studies on coefficient of restitution of wood satisfy this bound.[31] Further, sliding was not observed at impact from the experiments we conducted. The rocking was captured with motion tracking to measure the kinetic energy over the course of the rocking. By comparing the peak angular velocities for each cycle, a true value for r was measured for initial angles of $\phi_0 = 22, 11, 6$ degrees. Values for r were determined by averaging over the first five cycles or until the block came to rest, whichever came first. This way, even if the rocking starts at a high angle, information of low angle rocking is involved in the result. The r value found was ≈ 0.6 for $\phi_0 = 22°$, ≈ 0.5 for $\phi_0 = 11°$, and ≈ 0.25 for $\phi_0 = 6°$ and can be found in Figure A2. While the r values for the higher initial angles are similar, the r value for $\phi_0 = 6°$ is much lower. The angle measurements became more difficult at lower angles so the higher angle results are more reliable.

With values for r determined experimentally, the remaining question is how r and the C_{res}^N parameter in LS-DEM are related. To do this, the experiment was exactly replicated in the model for C_{res}^N ranging from 0.1 to 0.9 in increments of 0.02. For all materials it was determined that r is insensitive to the rocking angle and the coefficient of restitution, as shown in

Figure A2. Interestingly, the model predicts the *r* value that was found in experiments with the larger initial angles, but does not predict the *r* value obtained experimentally for small angles. Also, the model does not predict the value from the theory for inelastic collisions. The reason for this is suspected to be that the contact time is not sufficient for the damping. Regardless of the fact that the model does not capture the theoretical behavior of inelastic collisions at low coefficients of restitution, however, replicating the same *r* value at experiments for larger angles is a non-trivial result. Due to the insensitivity of this variable, its value was adjusted within the range of $0.3 - 0.5$ based on the block height variability of the tower sample. Higher levels of block height variability require more damping during tower sample preparation, so a lower value of the coefficient of restitution can be helpful.